

LOW-RANK LATENT MATRIX FACTOR-ANALYSIS MODELING FOR GENERALIZED LINEAR REGRESSION WITH HIGH-DIMENSIONAL IMAGING BIOMARKERS

BY YUZHE ZHANG¹, XU ZHANG^{2,*}, HONG ZHANG^{3,†} AND CATHERINE LIU^{4,‡}

¹*Department of Statistics and Finance, School of Management, University of Science and Technology of China, zyz2020@mail.ustc.edu.cn*

²*School of Mathematical Sciences, South China Normal University, *zhangx6690@gmail.com*

³*Department of Statistics and Finance, School of Management, University of Science and Technology of China, zhangh@ustc.edu.cn*

⁴*Department of Applied Mathematics, The Hong Kong Polytechnic University, macliu@polyu.edu.hk*

Medical imaging has been recognized as a phenotype associated with various clinical traits in diagnostics and prognosis of clinical trials and cancer studies. Imaging data used to be converted and stored into high-dimensional matrices in medical imaging data preprocessing. For the imaging predictor expressed in the form of a high-dimensional matrix variate, the mainstream tackling approaches tend to vectorize the matrix-valued predictor into a long regressor array plus a specific regularization scheme. Such vectorization may suffer the loss of information of intrinsic structure. Motivated by the cutting-edge matrix factor analysis modeling, we propose a new latent matrix factor generalized regression tool named FamGLM, which relates a scalar treatment outcome with predictors including imaging variate. The FamGLM enjoys high prediction capability since the extracted matrix factor score refines the structural effect of the matrix-valued predictor and circumvents over dimension reduction. Inspired by 2nd-order tensor principal component analysis, we develop a matrix SVD-based estimation procedure and algorithm through generalized low rank approximation of matrices, which has a much lower computation cost compared with existing statistical approaches. The proposed FamGLM also achieves higher prediction capability than existing methods. In numerical analysis, we evaluate the finite sample performance of FamGLM in classification and prediction compared with existing statistical approaches under various GLM scenarios. The FamGLM outperforms in discriminant power in analysis of a COVID-CT image data set.

1. Introduction. High-dimensional imaging data are often encountered in biometry and epidemiology as a companion of contemporary medical acquisition technologies. Imaging biomarkers are playing an important role in aiding diagnostics, prognosis, medical care plan, and monitoring of treatment outcomes in clinical trials and a wide range of medical studies (Suetens, 2017). There has arising research interest in tackling the image predictor in the past decade (Zhou et al. (2013); Ding and Cook (2018); Li and Zhang (2021); among others). In this paper, we propose a latent factor score regression to relate scalar clinical traits of the disease and the imaging predictor by the cutting-edge matrix factor analysis modeling technique.

Our work is motivated by discriminating infection of COVID-19 subjects from their chest computed tomography (CT) scanning slice images (Yang et al., 2020). CT is outpatient and affordable, thus preferred in most medical cares with Magnetic Resonance Imaging (MRI) as

Keywords and phrases: Latent factor score regression, Low rank approximation, Imaging reconstruction, Matrix variate, COVID-19.

an adjunct diagnostic tool. CT is a 3D imaging modality, also called a 3rd-order tensor, which can show a tumor's shape and size. The scanning slices of CT imaging are in axial, sagittal, and dorsal dimensions, corresponding to horizontal, lateral and frontal slices, respectively, in a tensor slicing (Kolda and Bader, 2009). Each slice image (2D image or 2nd-order tensor), is a matrix with entries being pixels that correspond to a voxel with certain thickness. Each pixel is assigned a numeric value reflecting the grayness (brightness) or color (hue, saturation and brightness). In general, the tumorous lesions may light up in the slice image (sometimes with contrast dye or agents). Axial scanning is the most straightforward acquisition mode and possibly is the most popular mode (Suetens, 2017). Therefore, axial slices of CT would be considered in general, and so are in the preprints of COVID-19 pandemic studies, and in the format of JPEG or PNG though.

The 3D imaging either has counterpart of 3rd-order tensor or has surrogate of matrix (2nd-order tensor) in medical data analytics, the latter of which is our target in this project, that is, the collection of 3D imaging data is represented as collection of high-dimensional matrices. There is rich literature in investigating how to cope with 2D or 3D image predictor so as to look into its influence on the treatment outcome in the past decade. The general idea focuses on dimension/dimensionality reduction of the tensor or matrix image predictor into a manageable low rank level, and one still hopes to preserve the inherent structural information meanwhile. We summarize existing methods dealing with 2D or 3D imaging predictor into three main categories according to the dimension/dimensionality reduction techniques. The first line of work may be the mainstream which is to vectorize the multiway array (another name for tensor) or matrix variate into a long vector and give various penalties. Under the framework of the GLM, representative works are to turn tensor regression by tensor decomposition schemes or matrix regression into multivariate regression plus proper regularization processes (Zhou et al. (2013); Zhou and Li (2014); Li and Zhang (2021); among others). For the specific logistic GLM, the rank-1 approximation applied in (Hung and Wang, 2013; Fang and Yi, 2021) is a special case of CP-decomposition for tensor (Kolda and Bader, 2009). The second line of research is to incorporate the hidden structure of the matrix variate by principal component (PC) decomposition (Caffo et al., 2010; Jiang et al., 2020). The third is to address the problem from sufficient dimension reduction to form the central dimension folding subspace (Li et al. (2010); Ding and Cook (2014); among others) but not lead to regression. It is noticed that there is also a branch of work that studies regression with the matrix-valued response and possible matrix-valued predictor through dimension folding (Li and Zhang, 2017; Ding and Cook, 2018).

The aforementioned vectorization or PC decomposition battling with image predictors may reduce dimension/dimensionality overly. For example, in dealing with matrix variate as the surrogate of image, one may ignore the interrelationship among rows or columns, or overlook the interrelated structural information between rows or between columns. This urges new solutions that respect the geometry inherent to the inner structure of the images. Thereafter, we focus on matrix-variate regression with flexible response coming out of the exponential distribution family. We consider inducing matrix factor analysis in that this tool is known of high interpretability and powerful extraction capability of hidden structure. From the insight of matrix factor analysis modeling, we propose a novel latent matrix factor generalized linear model named FamGLM, which associates the treatment outcome that may be discrete with structural regressors extracted from the matrix-valued image predictor. We first extract a set of low-dimensional common fundamental matrix factors factorized from the observed matrix-valued covariates based on a specific interaction matrix factor model. Next, this set of low-dimensional latent factor matrices is utilized as the input features to be linked with the treatment outcome of any type from the exponential distribution family. In this way, the original matrix structure can be preserved in a low-dimensional GLM to conduct tasks including regression and prediction.

The proposed modeling takes the advantage of factor analysis that a much less number of latent factors can characterize the correlation among a large number of multivariates accurately so that we can implement regression and prediction. In FamGLM, the matrix-valued predictor may have a high dimension in the sense that the row and column numbers can be very large. Such latent matrix factor regression modeling is quite new in analyzing generalized linear models involving imaging predictor, as we have not found any analogue in the published literature yet, to the best of our knowledge. Nevertheless, we admit that it is motivated from the latest development of factor analysis modeling in time series. Early nonlinear factor analysis modeling mainly dealt with factorization of vector (Lawley and Maxwell, 1962), in which the vector is represented by a few common vector factors, and the coordinate of loading matrix represents the interconnection of a coordinate of the vector on the coordinate of the common vector factor. Bai (2003) derived the initial and delicate statistical inference for the vector linear factor model in time series. However, Bai’s vector factor model looks as if it only handles the matrix-variate by rows or columns separately. Later, Wang et al. (2019) presented an interaction or bilinear-form matrix factor model that jointly takes the interconnection among rows and columns into account with large scale time series data setting, which limits its application owing to the strong assumption of white noise. The nonlinear factorization spirit of this model will still be a sharp weapon out of the temporal framework, which plays an important role to retain the intrinsic matrix structure in coping with independently observed matrix-valued data. Thus, further investigation is driven for independent or weakly dependent large scale data (Chen and Fan, 2021; Yu et al., 2021).

Besides the simple and straightforward modeling, we also contribute a complete FamGLM estimation methodology, which has two significant advantages: efficient computational performance and precise prediction capability, over existing working models for GLM with high-dimensional imaging predictors, including tensor regression series such as CPTR (Zhou et al., 2013), SVDTR (Zhou and Li, 2014) and TTR (Li et al., 2018). On one hand, the much less computation cost is owing to much less complicated iteration. FamGLM modeling directly extracts the low-rank latent factor score matrices from the original matrix observations in lieu of complicated iteration. Our estimation procedure applies 2DPCA, which is a principal component analysis tool for 2nd-tensors (Ye, 2005; Zare et al., 2018). The other way around, for CPTR and TTR, their estimation procedures follow the line of the classical optimization algorithm, named block relaxation (Lange et al., 2010), with the spirit that, a GLM should be fitted in each iteration in order to maximize the log likelihood function; for SVDTR, the estimation procedure is under the framework of Nesterov algorithm to solve the non-convex regularization problem (Beck and Teboulle, 2009). In summary, the computational complexity caused by various regularization schemes leads to indispensable iterations in solving optimization subproblems for algorithms of CPTR, SVDTR and TTR. On the other hand, the building of estimation procedures of FamGLM is based on GLRAM approach (Ye, 2005). GLRAM, which is categorized as a 2DPCA (Zare et al., 2018), is indeed a matrix incremental version of traditional vector SVD to alleviate the expensive SVD computation, and yet outperforms the vector SVD in view of compression ratio, the percentage of space saved by the low rank approximations to store the data. The essential difference between SVD and GLRAM is that GLRAM applies a bilinear transformation on the data, which keeps the structure invariant, and hence is particularly appropriate for imaging data in matrix form in terms of tasks of image compression and retrieval. The other way round, the tactic of CPTR and TTR is to break the structure by taking kind of tensor decomposition, incurring loss of structural information.

The rest of this paper is organized as follows. Section 2 formulates the latent factor generalized linear model and develops estimation procedure and algorithm for implementation of estimation. Section 3 displays the finite sample performance of FamGLM compared with several existing methods. FamGLM is also evaluated on COVID-19 CT image dataset in Section 4. Some discussion about the extension of FamGLM is illustrated in Section 5.

2. Latent-factor Generalized Linear Model. Let Y be the response variable that comes from the exponential family of distributions. The classical GLMs with canonical links include general models such as the normal linear regression, the logistic regression, and the Poisson regression. Let (\mathbf{X}, \mathbf{v}) be the covariates, where $\mathbf{X} \in \mathbb{R}^{p_1 \times p_2}$ and $\mathbf{v} \in \mathbb{R}^m$ are the matrix-valued and vector-valued covariates respectively. Through a prespecified link function $g(\cdot)$, the systematic mean regression part is connected with the conditional mean of the response given covariates. Recall that the straightforward generalized linear model that vectorizes the matrix-valued predictor has the conventional representation below,

$$(1) \quad g\{E(Y|\mathbf{X}, \mathbf{v})\} = \gamma + \eta^\top \text{vec}(\mathbf{X}) + \beta^\top \mathbf{v},$$

where $\text{vec}(\cdot)$ represents the vectorization operator by stacking \mathbf{X} column by column as a $p_1 p_2$ -vector, γ is the intercept term, $\eta \in \mathbb{R}^{p_1 p_2}$ may be a long vector or order-1 tensor, and $\beta \in \mathbb{R}^m$ is the coefficient vector.

An intuitive illustration of model (1) is that the (i, j) element of \mathbf{X} possesses its own effect $\eta_{i+p_1(j-1)}$ on the response, and the k th element of \mathbf{v} has its own effect β_k on the response. Equation (1) in Zhou and Li (2014) is the same with model (1) since $\langle \mathbf{B}, \mathbf{X} \rangle = \langle \text{vec}(\mathbf{B}), \text{vec}(\mathbf{X}) \rangle$, where $\langle \cdot, \cdot \rangle$ represents the inner product of two matrices. Equation (3) of Zhou et al. (2013) reduces to model (1) for the order-2 tensor with η being the tensor regression coefficient. Equation (1.1) in Hung and Wang (2013) reduces to a special case of model (1) under logit link function and $\mathbf{v} = \mathbf{0}$.

2.1. Model formulation. Nowadays, as the data volume becomes larger and larger, \mathbf{X} is often of high dimensionality, that is, p_1 and p_2 are very large. If we simply stack the covariate matrix into a vector to fit GLM, relevant information may be lost, and the problem of inefficiency will arise. Under this circumstance, motivated by factor analysis, we believe that the matrix-valued covariate \mathbf{X} is controlled by the global latent matrix factor of low dimension. Following this idea, we propose the FamGLM model

$$(2) \quad \begin{cases} g\{E(Y|\mathbf{Z}, \mathbf{v})\} = \gamma + \alpha^\top \text{vec}(\mathbf{Z}) + \beta^\top \mathbf{v}, \\ \mathbf{X} = \mathbf{R}\mathbf{Z}\mathbf{C}^\top + \mathbf{E}, \end{cases}$$

where $\mathbf{Z} \in \mathbb{R}^{k_1 \times k_2}$ ($k_1 \ll p_1$ and $k_2 \ll p_2$) is the unobserved common fundamental matrix factor, $\mathbf{E} \in \mathbb{R}^{p_1 \times p_2}$ is the random error matrix, $\alpha \in \mathbb{R}^{k_1 k_2}$ is the coefficient vector corresponding to $\text{vec}(\mathbf{Z})$, row factor loading matrix $\mathbf{R} \in \mathbb{R}^{p_1 \times k_1}$ reflects the dependencies between rows and column factor loading matrix $\mathbf{C} \in \mathbb{R}^{p_2 \times k_2}$ represents the dependencies between columns, with k_1 and k_2 being the numbers of row and column factors respectively. Without loss of generality, we still follow the same notation of γ and β in (1) since the meaning is invariant. In model (2), the global latent matrix factor \mathbf{Z} inherits the interaction effects or the co-movement of rows and columns of \mathbf{X} . Hence $\text{vec}(\mathbf{Z})$ becomes an excellent structural regressor vector that catches the intrinsic interrelationship among rows and columns.

With sample data set $\{(Y_i, \mathbf{X}_i, \mathbf{v}_i)\}_{1 \leq i \leq n}$, the interpretation of model (2) can be demonstrated. On one hand, one can view the factor model part in model (2) as

$$x_{kj,i} = \sum_{h,l} r_{kh} z_{hl,i} c_{jl} + e_{kj,i},$$

where $x_{kj,i}$ is the (k, j) element of the i th matrix variate observation \mathbf{X}_i , r_{kh} is the (k, h) element of the row loading matrix \mathbf{R} , c_{jl} is the (j, l) element of the column loading matrix \mathbf{C} , $z_{hl,i}$ is the (h, l) element of the i th latent matrix factor, and $e_{kj,i}$ is the (k, j) element of the i th error matrix \mathbf{E} . Each summand $r_{kh} z_{hl,i} c_{jl}$ can be interpreted as the latitudinal contribution from the k th row to the h th row, and the longitudinal contribution of column j to column l

in the interaction effect from row h to column l . The total volume $x_{kj,i}$ is the aggregation of the interaction volumes from row k to column j through all the latent factor scores.

On the other hand, for the GLM part, the regressor vector $\text{vec}(\mathbf{Z})$, which replaces the original matrix-variate predictor \mathbf{X} , plays a critical role in the latent matrix factor modeling in that it extracts and maintains the intrinsic information contained in the matrix-valued covariate \mathbf{X} . Meanwhile, the parameters to be estimated reduce significantly from $1 + p_1 p_2 + m$ to $1 + k_1 k_2 + m$. Once we can estimate the latent matrix factor \mathbf{Z} accurately, the low-dimensional GLM with latent factors vectorized as the regressors can be fitted effectively through the general methods.

2.2. Statistical Estimation Procedure. As an alternative to the traditional singular value decomposition based methods, the generalized low rank approximations of matrices (GLRAM) provides justification in optimization for iterations that are computationally much efficient (Ye, 2005). This is the cornerstone of our estimation procedure. For model (2), the key point is to estimate the latent matrix factor \mathbf{Z} . In this subsection, we develop the methodology to estimate matrix factors $\{\mathbf{Z}_i\}_{1 \leq i \leq n}$ from observations $\{\mathbf{X}_i\}_{1 \leq i \leq n}$. Note that we do not make any assumptions on the error term \mathbf{E} in (2).

For any invertible matrices $\mathbf{H}_1 \in \mathbb{R}^{k_1 \times k_1}$ and $\mathbf{H}_2 \in \mathbb{R}^{k_2 \times k_2}$, we can see that $\{\mathbf{R}, \mathbf{C}, \mathbf{Z}\}$ and $\{\mathbf{R}\mathbf{H}_1, \mathbf{C}\mathbf{H}_2, \mathbf{H}_1^{-1}\mathbf{Z}(\mathbf{H}_2^{-1})^\top\}$ can result in the same model. For the sake of identifiability, we assume the constraints on model (2)

$$(3) \quad \mathbf{R}^\top \mathbf{R} = p_1 \mathbf{I}_{k_1}, \mathbf{C}^\top \mathbf{C} = p_2 \mathbf{I}_{k_2}.$$

In order to estimate \mathbf{R} and \mathbf{C} , we minimize the Frobenius norm of residual matrix \mathbf{E} , which may be understood as the reconstruction error of the approximation of $\mathbf{R}\mathbf{Z}\mathbf{C}^\top$ to \mathbf{X} in the machine learning community. The objective function under the Frobenius norm can be formulated as

$$(4) \quad (\hat{\mathbf{R}}, \hat{\mathbf{C}}) = \arg \min_{\substack{\mathbf{R}^\top \mathbf{R} = p_1 \mathbf{I}_{k_1} \\ \mathbf{C}^\top \mathbf{C} = p_2 \mathbf{I}_{k_2}}} \frac{1}{p_1 p_2 n} \sum_{i=1}^n \|\mathbf{X}_i - \mathbf{R}\mathbf{Z}_i\mathbf{C}^\top\|_F^2,$$

where p_1 and p_2 may both be sufficiently large. Generally, we cannot give an explicit expression of $\hat{\mathbf{R}}$ and $\hat{\mathbf{C}}$. Notice that, under the assumptions that p_1, p_2 and n are finite and the observations are identically and independently distributed, if one reparameterizes $\tilde{\mathbf{R}} = \mathbf{R}/\sqrt{p_1}$, $\tilde{\mathbf{C}} = \mathbf{C}/\sqrt{p_2}$, $\tilde{\mathbf{Z}}_i = \sqrt{p_1 p_2} \mathbf{Z}_i$, then the optimization problem (4) becomes identical with formulation equation (1) in Ye (2005). This observation drives us to compute optimal \mathbf{R} and \mathbf{C} to solve our minimization problem (2) along the line of computing optimal \mathbf{L} and \mathbf{R} for their minimization problem (1) in Ye (2005). The construction of \mathbf{M}_L and \mathbf{M}_R in Theorem 3.3 of Ye (2005) further inspires our optimal solution of \mathbf{R} and \mathbf{C} to the minimization problem (4).

Let \mathbf{M}_R and \mathbf{M}_C be the row and column sample version second-order moment matrices of \mathbf{X} , respectively. One may also center these two matrices to obtain the row and column covariance matrices of \mathbf{X} without loss of generality. Notice that \mathbf{M}_R and \mathbf{M}_C in our minimization problem (4) play the same role as \mathbf{M}_L and \mathbf{M}_R in Ye's optimization problem (1). Under our constraints (3) for minimization problem (4), the i th matrix-valued predictor observation \mathbf{X}_i corresponds to $\mathbf{A}_i \mathbf{R}$ in Theorem 3.3 of Ye (2005), generating the estimators

$$(5) \quad \hat{\mathbf{M}}_R = \frac{1}{n p_1 p_2} \sum_{i=1}^n \mathbf{X}_i \mathbf{X}_i^\top, \quad \hat{\mathbf{M}}_C = \frac{1}{n p_1 p_2} \sum_{i=1}^n \mathbf{X}_i^\top \mathbf{X}_i,$$

respectively. That is, we estimate \mathbf{M}_R and \mathbf{M}_C by their sample versions directly.

Next we apply the spectral approach on the sample row and column second-order moment matrices. Let \mathbf{Q}_R be the matrix with columns being the eigenvectors of $\hat{\mathbf{M}}_R$ corresponding to

the first k_1 largest eigenvalues. Then, $\hat{\mathbf{R}}$ is of order $p_1 \times k_1$ up to a multiplier $\sqrt{p_1}$ on \mathbf{Q}_R . Let \mathbf{Q}_C be the matrix with columns being the eigenvectors of $\hat{\mathbf{M}}_C$ corresponding to the first k_2 largest eigenvalues. Then, $\hat{\mathbf{C}}$ is of order $p_2 \times k_2$ up to a multiplier $\sqrt{p_2}$ on \mathbf{Q}_C . In practice, the number of row factors k_1 and column factors k_2 are usually unknown. Visually, one can use the scree plot to calculate two estimators. Let $\hat{\lambda}_{1,1} \geq \hat{\lambda}_{1,2} \geq \dots \geq \hat{\lambda}_{1,p_1} \geq 0$ be the descending eigenvalues of $\hat{\mathbf{M}}_R$, and $\hat{\lambda}_{2,1} \geq \hat{\lambda}_{2,2} \geq \dots \geq \hat{\lambda}_{2,p_2} \geq 0$ be the descending eigenvalues of $\hat{\mathbf{M}}_C$, respectively. Then, the general estimates of k_1 and k_2 are

$$(6) \quad \hat{k}_1 = \arg \max_{1 \leq j \leq \lceil p_1/2 \rceil} \frac{\hat{\lambda}_{1,j}}{\hat{\lambda}_{1,j+1}}, \quad \hat{k}_2 = \arg \max_{1 \leq j \leq \lceil p_2/2 \rceil} \frac{\hat{\lambda}_{2,j}}{\hat{\lambda}_{2,j+1}}.$$

Numerically, these two estimators can be derived through a similar eigenvalue ratio estimator as described in [Lam and Yao \(2012\)](#).

Once $\hat{\mathbf{R}}$ and $\hat{\mathbf{C}}$ are obtained, \mathbf{Z}_i can be estimated using $\hat{\mathbf{Z}}_i = \hat{\mathbf{R}}^\top \mathbf{X}_i \hat{\mathbf{C}} / (p_1 p_2)$. By far, we have the data set $\{(Y_i, \hat{\mathbf{Z}}_i, \mathbf{v}_i)\}_{1 \leq i \leq n}$ to model FamGLM presented in (2) which treats Y_i as the response and $(\text{vec}(\hat{\mathbf{Z}}_i), \mathbf{v}_i)$ as covariates to conduct regression and classification tasks.

We conclude our algorithm to model FamGLM as follows:

Algorithm 1 FamGLM

Require: Response variable $\{Y_i\}_{i=1}^n$, matrix-valued covariates $\{\mathbf{X}_i\}_{i=1}^n$, vector-valued covariates $\{\mathbf{v}_i\}_{i=1}^n$, $1 \leq i \leq n$.

- 1: Calculate matrix $\hat{\mathbf{M}}_R$ and $\hat{\mathbf{M}}_C$ according to (5).
 - 2: Choose the number of row factors k_1 and column factors k_2 according to (6).
 - 3: Calculate loading matrices $\hat{\mathbf{R}}$ and $\hat{\mathbf{C}}$: $\hat{\mathbf{R}}$ is $\sqrt{p_1}$ times the top k_1 eigenvectors of $\hat{\mathbf{M}}_R$, $\hat{\mathbf{C}}$ is $\sqrt{p_2}$ times the top k_2 eigenvectors of $\hat{\mathbf{M}}_C$.
 - 4: Calculate latent factor matrices $\hat{\mathbf{Z}}_i = \hat{\mathbf{R}}^\top \mathbf{X}_i \hat{\mathbf{C}} / (p_1 p_2)$.
 - 5: Model GLM using the data set $\{(Y_i, \text{vec}(\hat{\mathbf{Z}}_i), \mathbf{v}_i)\}_{1 \leq i \leq n}$.
-

Remark 1: It follows the same line to estimate the row and column loading matrices \mathbf{R} and \mathbf{C} in existing literature within the interaction factor model. The estimation of \mathbf{M}_R and \mathbf{M}_C is the stone threshold in the series of research concerning the interaction matrix factor model for large-scale time series data. [Wang et al. \(2019\)](#) preassigned the auto-cross-covariances to construct \mathbf{M}_R and \mathbf{M}_C under the dependent time series data setting. [Chen and Fan \(2021\)](#) provided a tradeoff between the first-order and the second-order moments in their estimation construction of \mathbf{M}_R and \mathbf{M}_C for independent or weak dependent subjects. [Yu et al. \(2021\)](#) projected along the direction of row or column so as to separate the remainders. For our proposed factor-analysis generalized linear regression, our estimates $\hat{\mathbf{M}}_R$ and $\hat{\mathbf{M}}_C$ are intuitive and concise since we assume that the observations of subjects are independent. The choice of $\hat{k}_i, i = 1, 2$, i.e., the number of columns of the estimate of \mathbf{M}_R and \mathbf{M}_C , are identical for the common interaction matrix variate factor model ([Wang et al., 2019](#); [Chen and Fan, 2021](#); [Yu et al., 2021](#)).

Remark 2: Consider evaluating the accuracy of prediction and association of the proposed FamGLM tackling matrix-valued predictor. We illustrate this with a logistic regression model for a binary outcome, and use the area under the ROC curve (AUC) as an accuracy metric ([Liu et al., 2011](#)):

$$AUC = \Pr \{h(\mathbf{Z}, \mathbf{v}) > h(\mathbf{Z}', \mathbf{v}')\}.$$

Here $h(\cdot)$ is the regression part of the FamGLM model with the dichotomous response, (\mathbf{Z}, \mathbf{v}) is the covariates of the group with response $Y = 1$, and $(\mathbf{Z}', \mathbf{v}')$ is the covariates of the group with response $Y = 0$.

3. Simulation Studies. In this section, the finite sample performance of the proposed FamGLM is evaluated through extensive numerical studies. First, in Subsection 3.1, we hope to examine the suitability of the association of factor scores of the matrix-valued predictor with a kind of response, working to replace the conventional generalized linear model (1). Specifically, we demonstrate and compare within the popular logistic regression setting to see the validity of FamGLM. Second, in Subsection 3.2, the predictive power of FamGLM is compared with several existing tensor regression methods including CP Tensor Regression (Zhou et al., 2013), SVD Tensor Regression (Zhou and Li, 2014), and Tucker Tensor Regression (Li et al., 2018), which are abbreviated as CPTR, SVDTR, and TTR thereafter, respectively, for the response types of binary, normal and Poisson. We admit the CPTR model with CP decomposition using $R = 1$, and TTR model with Tucker decomposition using $(R_1, R_2) = (1, 2)$. We implement CPTR, SVDTR, and TTR using the Matlab toolbox TensorReg (<https://hua-zhou.github.io/TensorReg/>), and our own FamGLM is implemented in R language and the R code for simulation studies can be downloaded from GitHub (<https://github.com/zyz0000/FamGLM/>). Third, in Subsection 3.3, we perform a simulation under close setting of the real data analyzed in Section 4 to evaluate discriminant of FamGLM. We also include comparison with MV-logistic model (Hung and Wang, 2013) since we diagnose whether a subject is COVID-19 infected or not based on the CT imaging.

3.1. *The analysis of goodness of fit.* We compare discriminant capability between conventional logistic model (1) and the proposed FamGLM based on simulated data. For the latent matrix factor \mathbf{Z} , let the dimension of global latent matrix factor \mathbf{Z} be $(k_1, k_2) = (3, 3)$ and $\text{vec}(\mathbf{Z}) \sim MVN(\mathbf{0}, \mathbf{\Sigma})$, where $\Sigma_{ij} = 0.5^{|i-j|}$, $1 \leq i, j \leq k_1 k_2$. The entries of true loading matrices \mathbf{R} and \mathbf{C} are independently sampled from the uniform distribution $U(-\sqrt{p_1}, \sqrt{p_1})$ and $U(-\sqrt{p_2}, \sqrt{p_2})$. Each entry of the noise matrix \mathbf{E} is generated from a standard normal distribution $N(0, 1)$. The matrix-valued covariate \mathbf{X} is generated according to $\mathbf{X} = \mathbf{R}\mathbf{Z}\mathbf{C}^\top + \mathbf{E}$. We generate binary response Y from Bernoulli distribution with the probability of occurrence p and logit link to obtain the mean regression, where $\text{logit}(p) = \mu = \gamma + \alpha^\top \text{vec}(\mathbf{Z})$, where $\gamma = 1$, $\alpha = (1, -1, 0.5\mathbf{1}_4^\top, -0.5\mathbf{1}_3^\top)^\top$, with $\mathbf{1}_n$ being an n -vector with coordinates all unit. Simulation results are obtained under sample size $n = 150, 300$, with the dimension of \mathbf{X} being $(p_1, p_2) = (12, 10), (20, 15)$, or $(20, 30)$.

For each scenario (p_1, p_2, n) , a training set and a validation set of equal sample size n are generated. The training set is used to train FamGLM and conventional logistic model and the validation set is used for evaluation. Note that the number of factors (\hat{k}_1, \hat{k}_2) are determined by equation (6) and thereafter. The cutoff value is chosen consistently to be 0.5. Based on 100 replicates of simulations, the average classification accuracy (CA) and the winning percentage (WP) are reported in Table 1. Evidently, FamGLM overwhelmingly outperforms the conventional logistic in terms of both accuracy and WP. Specifically, the accuracy gains of FamGLM range from 0.117 to 0.269, depending on the parameter combinations. The WPs are uniformly 1 in all the simulation scenarios, which implies that FamGLM perfectly categorizes the association between response and matrix-valued covariates.

The ROC curves under three different settings of (p_1, p_2) are shown in Figure 1. The ROC curve of FamGLM is much higher than the counterpart of the conventional logistic model. As a result, the AUC of FamGLM is much higher than the conventional logistic model. It can be concluded that FamGLM outperforms the conventional logistic model in the simulation situations.

3.2. *Finite sample performance of FamGLM.* We aim to compare the predictive performance of four models: FamGLM, CPTR, SVDTR, and TTR, which have been referred

TABLE 1
 CA of conventional logistic/FamGLM and WP of FamGLM for different scenarios of (p_1, p_2) and $n = 150, 300$.

(p_1, p_2)	$n = 150$			$n = 300$		
	Logistic	FamGLM	WP	Logistic	FamGLM	WP
(12,10)	0.581	0.763	1.00	0.654	0.771	1.00
(20,15)	0.504	0.765	1.00	0.505	0.769	1.00
(20,30)	0.517	0.767	1.00	0.506	0.775	1.00

1 Classification accuracy (CA): the proportion of correctly predicted observation to the total observations.

2 Winning percentage (WP): the percentage of FamGLM with higher classification accuracy than the conventional logistic model.

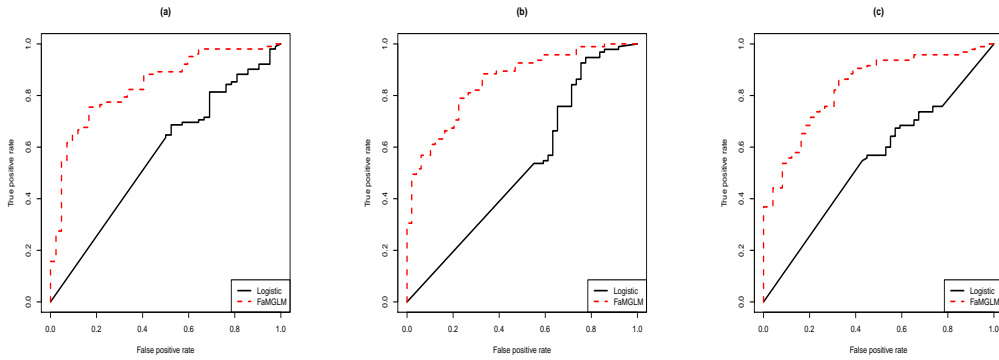


FIG 1. The ROC curve of FamGLM vs. logistic model under (a) $p_1 = 12, p_2 = 10$; (b) $p_1 = 20, p_2 = 15$; (c) $p_1 = 20, p_2 = 30$.

to at the beginning of Section 3. We choose (p_1, p_2) among $(20, 20)$, $(20, 50)$ and $(50, 50)$, and let sample size be $n = \rho p_1 p_2$, $\rho \in \{0.5, 1, 1.5, 2\}$. The procedure to generate matrices \mathbf{R} , \mathbf{Z} , \mathbf{C} , \mathbf{E} is exactly the same with the one described in Subsection 3.1. In addition, we take the usual vector of covariates \mathbf{v} into consideration for model (2), where $\mathbf{v} = (v_1, v_2, v_3)^\top \sim MVN(\mathbf{0}, \mathbf{I}_3)$.

Denote the mean regression $\mu = \gamma + \alpha^\top \text{vec}(\mathbf{Z}) + \beta^\top \mathbf{v}$, where $\gamma = 1$, $\alpha = (2, -2, \mathbf{1}_3^\top, -\mathbf{1}_4^\top)^\top$ and $\beta = \mathbf{1}_3$. We then generate the response through three submodels of GLM: for binomial model, $Y \sim \text{Bernoulli}(p)$, with the link function $g(x) = \log\{x/(1-x)\}$ and $p = \text{logit}^{-1}(\mu)$; for normal model, $Y \sim N(\mu, 1)$, with the canonical link function $g(x) = x$; for Poisson model, $Y \sim \text{Poisson}(\max(\exp(\mu), 1))$, with link function $g(x) = \log(x)$, where the $\max(\cdot)$ operator aims to prevent the possible numerical instability for the case when μ is very small.

In order to compare the four models mentioned above, the evaluation metrics are calculated via five-fold cross validation. We conduct 100 replicates in total. For the single tuning parameter in model SVDTR, the tuning parameter λ is selected on another extra independent validation set with sample size equals to 200, whose data generation procedure is the same as the one to generate a training set. For SVDTR, one needs to adjust one tuning parameter λ ; for TTR and CPTR, there is an additional tuning parameter of penalty type.

3.2.1. *FamGLM for the simulated normal response.* The metrics for the normal model are root mean squared error (RMSE), mean absolute error (MAE). The boxplots of RMSE and MAE under different combinations of $\{(p_1, p_2), \rho\}$ are displayed in Figure 2. It is clear that both RMSE and MAE decrease when the sample size becomes larger for fixed (p_1, p_2) ;

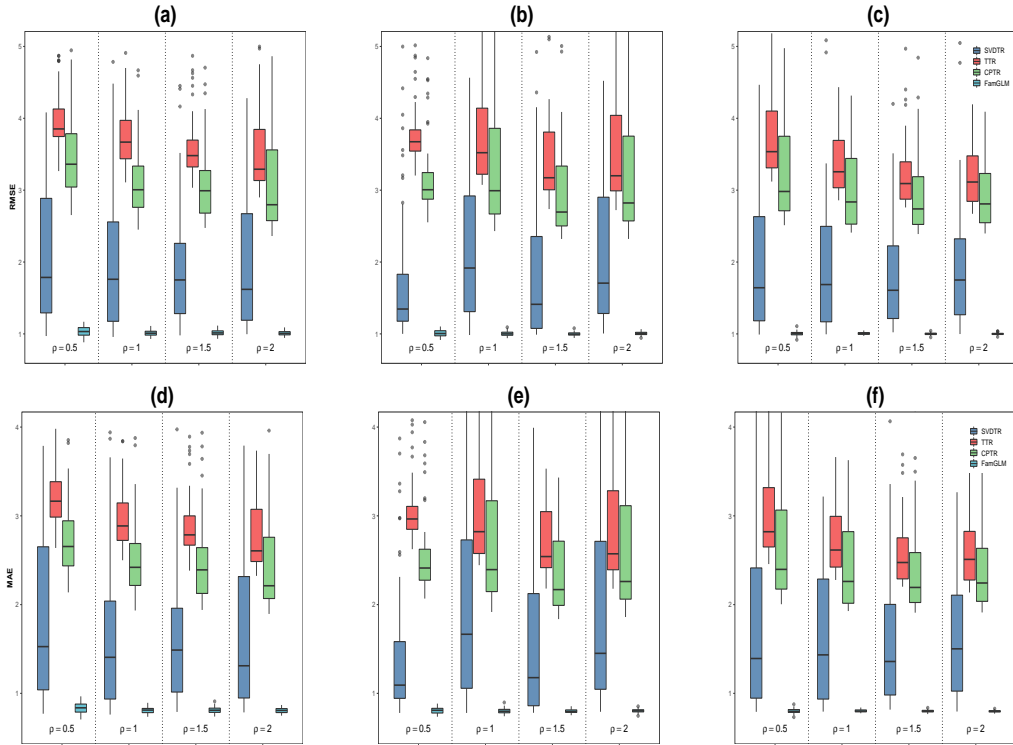


FIG 2. RMSE of four models under normal model: (a) $p_1 = 20, p_2 = 20$; (b) $p_1 = 20, p_2 = 50$; (c) $p_1 = 50, p_2 = 50$; MAE of four models under normal model: (d) $p_1 = 20, p_2 = 20$; (e) $p_1 = 20, p_2 = 50$; (f) $p_1 = 50, p_2 = 50$.

meanwhile, it can be seen that the RMSE of FamGLM are the smallest among four models under all scenarios of $\{(p_1, p_2), \rho\}$, which indicates that FamGLM achieves the smallest prediction volatility.

3.2.2. *FamGLM for the simulated binomial response.* We report five metrics as performance measurements for the binomial model, including CA, Kappa coefficient, AUC, sensitivity, and F1 score. These five metrics together represent comprehensive discriminant capability of a classifier. The cutoff value was fixed at 0.5 in calculating CA, Kappa, sensitivity, and F1 score. Kappa measures the interrater reliability, representing the extent to which the data collected in the study are correct representations of the variables measured. Sensitivity is the proportion of correctly predicted positive observations to all observations in the actual positive class. F1 score is a tradeoff between positive predictive rates and sensitivity. The boxplots of these five metrics under different scenarios of $\{(p_1, p_2), \rho\}$ are displayed in Figures 3 and 4. All these five metrics get closer to 1 when the sample size increases from $0.5p_1p_2$ to $2p_1p_2$. FamGLM outperforms significantly on classification accuracy, Kappa and sensitivity, but has similar performance on AUC and F1 score compared with SVDTR.

Figure 4 also shows the comparison of ROC curves. These three subplots illustrate that FamGLM (in solid line) and SVDTR (in dashed line) are comparable, and much better than TTR (in dash-dot line) and CPTR (in long dash line). We also observe that SVDTR may have weak advantage over FamGLM when p_1 and p_2 are both small ($(p_1, p_2) = (20, 20)$). When the false positive rate is smaller than 0.4, the partial AUC of FamGLM is larger than that of SVDTR. But when the false positive rate gets larger than 0.4, the partial AUC of both models becomes competitive. For the case $(p_1, p_2) = (20, 50)$, when the false positive rate is smaller than 0.3, the partial AUC of FamGLM is larger than that of SVDTR, whereas when the false

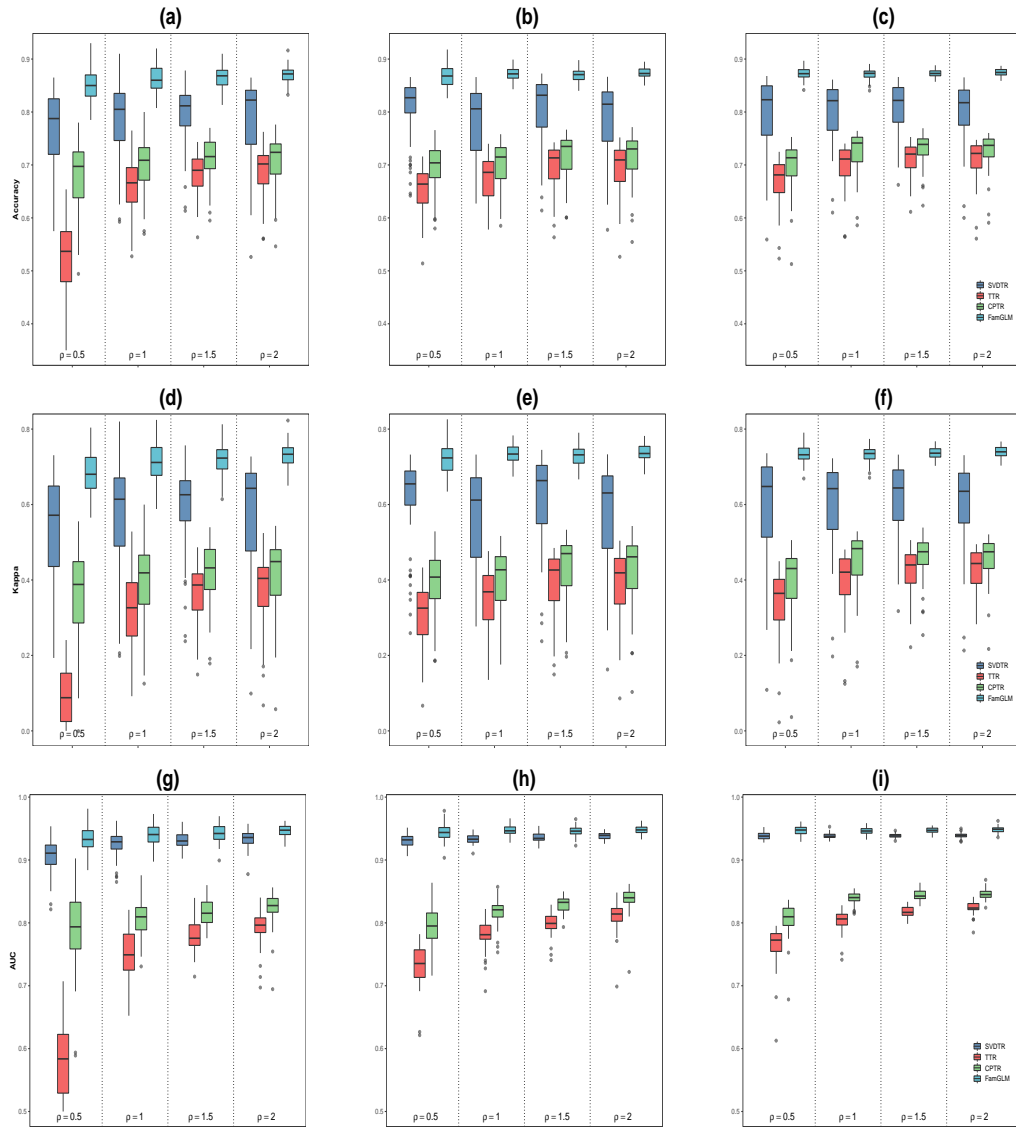


FIG 3. Classification accuracy of four models under binomial model: (a) $p_1 = 20, p_2 = 20$; (b) $p_1 = 20, p_2 = 50$; (c) $p_1 = 50, p_2 = 50$; Kappa of four models under binomial model: (d) $p_1 = 20, p_2 = 20$; (e) $p_1 = 20, p_2 = 50$; (f) $p_1 = 50, p_2 = 50$; AUC of four models under binomial model: (g) $p_1 = 20, p_2 = 20$; (h) $p_1 = 20, p_2 = 50$; (i) $p_1 = 50, p_2 = 50$.

positive rate gets larger than 0.3, the partial AUC of SVDTR has advantage over FamGLM. FamGLM performs slightly better than SVDTR when $(p_1, p_2) = (50, 50)$. Overall, FamGLM still performs the best among four models under binomial GLM submodel.

3.2.3. FamGLM for the simulated Poisson response. The metrics for the Poisson model are root mean squared error (RMSE), normalized mean squared error (NMSE) and mean absolute error (MAE). The boxplots of the three metrics under different scenarios of $\{(p_1, p_2), \rho\}$ are displayed in Figure 5. It is noticed that FamGLM achieves the smallest prediction volatility among four models because it gets the smallest RMSE, NMSE, and MAE under all settings of $\{(p_1, p_2), \rho\}$.

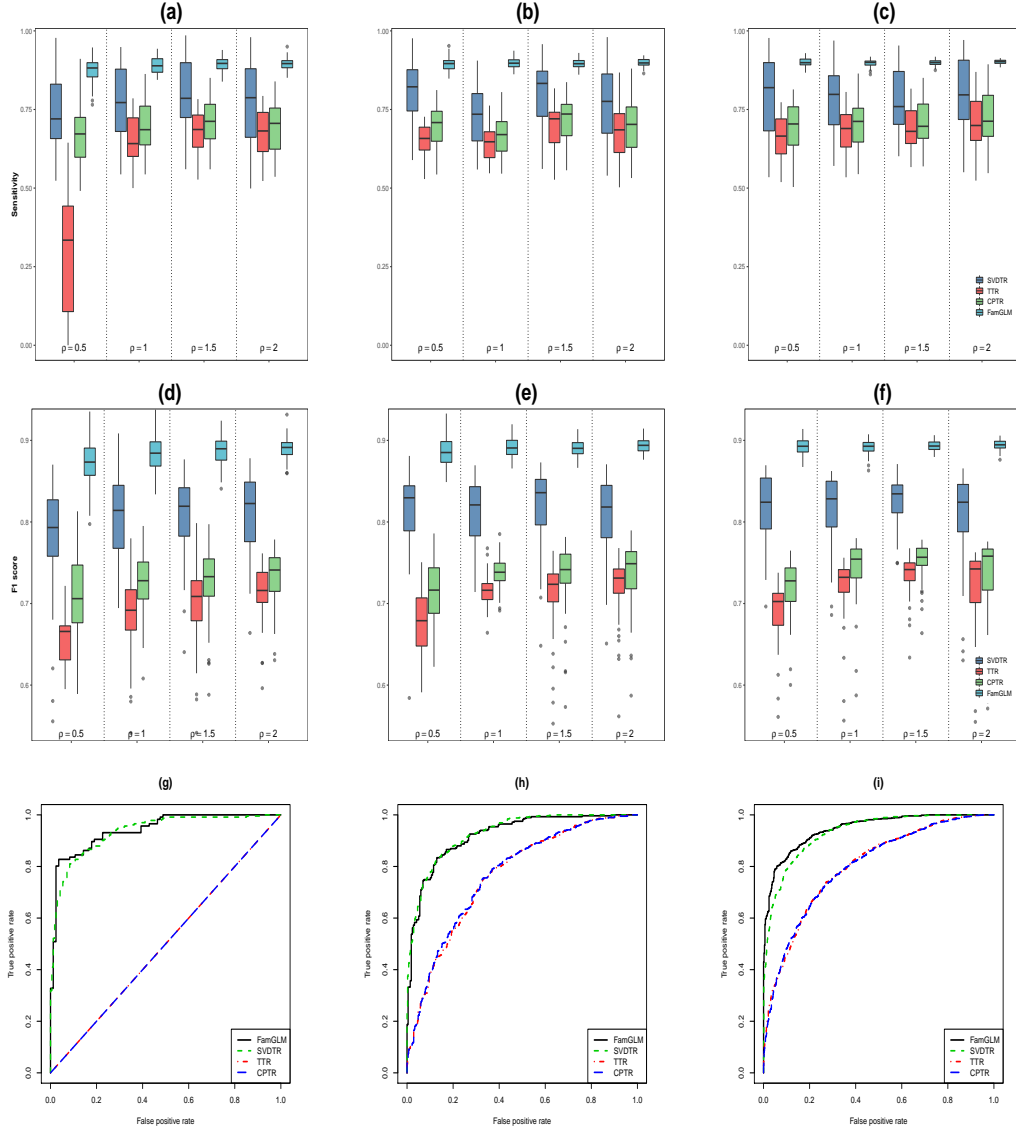


FIG 4. Sensitivity of four models under binomial model: (a) $p_1 = 20, p_2 = 20$; (b) $p_1 = 20, p_2 = 50$; (c) $p_1 = 50, p_2 = 50$; F1 score of four models under binomial model: (d) $p_1 = 20, p_2 = 20$; (e) $p_1 = 20, p_2 = 50$; (f) $p_1 = 50, p_2 = 50$; ROC curve of four models under binomial model: (g) $p_1 = 20, p_2 = 20$; (h) $p_1 = 20, p_2 = 50$; (i) $p_1 = 50, p_2 = 50$.

3.3. *FamGLM under the setting of COVID-CT Data Set.* This simulation scheme is inspired by the COVID-CT data set that we will analyze in the next section. In the COVID-CT data set, the sample size is $n = 746$, and the dimension of the observed matrix predictors is fixed with $(p_1, p_2) = (150, 150)$. The proportion of infection is about 47% based on the fact that there are 349 CT images of COVID-19 patients and 397 CT images of health subjects in the data set. In the simulation, we set the same parameter magnitudes for (n, p_1, p_2) . The procedure to generate matrices $\mathbf{R}, \mathbf{C}, \mathbf{E}$ follows what we do in Subsection 3.1. For the latent matrix factor \mathbf{Z} , let the dimension of global latent matrix factor \mathbf{Z} be $(k_1, k_2) = (3, 3)$ and $\text{vec}(\mathbf{Z}) \sim \text{MVN}(\phi, \Sigma)$, where $\phi = (1, 0.5, 1, -0.5, 1, 0.5, 1, -0.5, 1)^\top$, $\Sigma_{ij} = 0.5^{|i-j|}$, $1 \leq i, j \leq k_1 k_2$. Denote the mean regression $\mu = \gamma + \alpha^\top \text{vec}(\mathbf{Z})$, where $\alpha = (2, -2, \mathbf{1}_3^\top, -\mathbf{1}_4^\top)^\top$, $\gamma = \text{logit}(0.47) - \alpha^\top \phi = \text{logit}(0.47) - 0.5$, such that $\text{E}(\mu) = \gamma +$

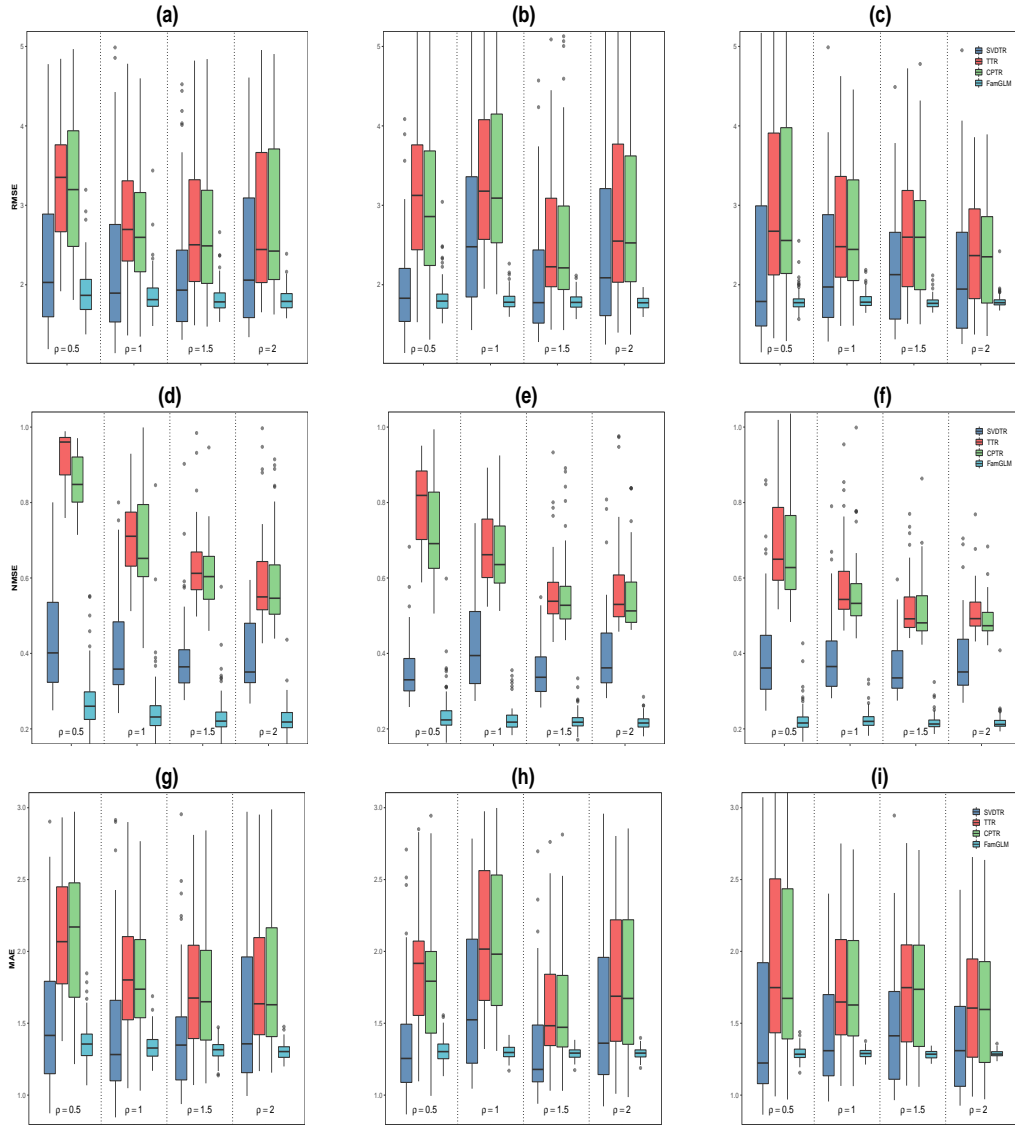


FIG 5. (a)-(c): RMSE of four models under Poisson model: (a) $p_1 = 20, p_2 = 20$; (b) $p_1 = 20, p_2 = 50$; (c) $p_1 = 50, p_2 = 50$; (d)-(f): NMSE of four models under Poisson model: (d) $p_1 = 20, p_2 = 20$; (e) $p_1 = 20, p_2 = 50$; (f) $p_1 = 50, p_2 = 50$; (g)-(i): MAE of four models under Poisson model: (g) $p_1 = 20, p_2 = 20$; (h) $p_1 = 20, p_2 = 50$; (i) $p_1 = 50, p_2 = 50$;

$\alpha^\top \mathbb{E} \{\text{vec}(\mathbf{Z})\} = 0.47$. We then generate the binary response by $Y \sim \text{Bernoulli}(p)$ and $p = \text{logit}^{-1}(\mu)$. Our comparison includes MVlogistic because it is specifically designed for binary response with matrix variate. We conduct 100 replicates in total, and the proportion of infected is 48.9%. We report the metrics for the binomial model, including classification accuracy, Kappa coefficient, AUC, sensitivity, and F1 score. Table 2 summarizes the mean and standard deviation of the five classification metrics mentioned above. FamGLM and SVDTR are competitive and overwhelmingly superior to the other three penalized methods, which cannot reach a satisfactory discriminant power. The possible reason is that (p_1, p_2) , the dimensionality of the matrices, is relatively high beyond the scope that these models can handle.

TABLE 2

The means (standard errors) of classification metrics based on 100 simulated COVID-CT datasets with five-fold cross validation.

	CA	Kappa	Sensitivity	AUC	FI score
FamGLM	0.855 (0.016)	0.708 (0.033)	0.853 (0.026)	0.936 (0.011)	0.851 (0.019)
SVDTR	0.846(0.014)	0.691(0.029)	0.841(0.021)	0.928(0.009)	0.842(0.016)
MVlogistic	0.501(0.050)	0.009(0.097)	0.575(0.145)	0.521(0.063)	0.482(0.096)
TTR	0.488(0.019)	0.000(0.000)	1.000(0.000)	0.500(0.000)	0.655(0.017)
CPTR	0.472(0.018)	0.000(0.000)	1.000(0.000)	0.500(0.000)	0.641(0.016)

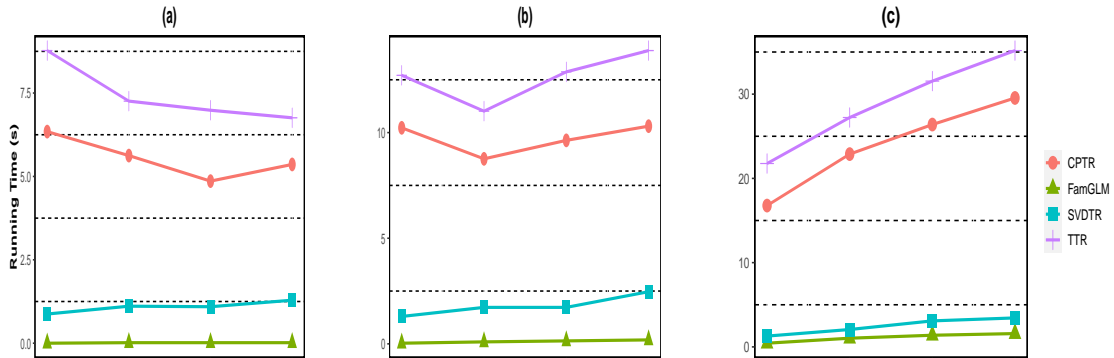


FIG 6. (a)-(c): Running time required for four models, including FamGLM (in chartreuse triangle), CPTR (in brown circle), SVDTR (in cyan square) and TTR (in blueviolet plus), to complete one replicate under different combination of (p_1, p_2) when ρ increases from 0.5 to 2: (a) $p_1 = 20, p_2 = 20$; (b) $p_1 = 20, p_2 = 50$; (c) $p_1 = 50, p_2 = 50$.

3.4. *Comparison of Computation Time.* In this subsection, we aim to give a direct comparison of computation time of FamGLM, CPTR (Zhou et al., 2013), SVDTR (Zhou and Li, 2014), and TTR (Li et al., 2018). The procedure to generate data follows exactly the same as that described in Subsection 3.2. We perform the runtime test procedure 100 times and report the median of the running time in Figure 6. The four models are all implemented by Matlab2019a, and the code is tested on a Windows10 laptop with Intel(R) Core(TM) i7-1065G7 CPU @ 1.30GHz and 16GB RAM. It can be seen that TTR and CPTR are far more time-consuming than FamGLM and SVDTR. Moreover, the running time of FamGLM does not increase significantly as (p_1, p_2) gets larger.

4. Real example: COVID-CT Data Set. The novel coronavirus or SARS-CoV2, also known as COVID-19, has increased greatly since the virus spread across the globe in spring 2020 and has caused millions of deaths all over the world until the end of 2020. Identifying and isolating patients infected with COVID-19 is an important step in managing this global pandemic. Many tests including image tests have been applied to diagnose and prevent the spread of COVID-19. Among them, chest computed tomography (CT) scans have been used for the purpose of screening and diagnosing quite popularly since it is noninvasive and of low risk (Kapoor et al., 2004). A chest CT scan combines a series of X-ray images taken from different angles around the chest and uses computer processing to create cross-sectional images (slices) of the chest.

We use an open-source chest CT data called COVID-CT, which was one of the largest publicly available COVID-19 CT scan datasets in the early pandemic. The COVID-CT dataset is available from <https://github.com/UCSD-AI4H/COVID-CT>. It has 349 COVID-19 positive CT scans and 397 negative CT scans in 2D grayscale images mainly in the format

of JPEG and PNG, which were manually selected from the embedded figures out of preprints on medRxiv2 and bioRxiv3, as well as some open source database. Experienced radiologist can still make accurate diagnosis from a single slice of low-quality CT images (Yang et al., 2020). In our methodology, we will apply our FA model technique to extract essential information from these degraded grayscale figures, in the sense that the number of bits per pixel and the resolution are negatively impacted. In Figure 7, Subfigures (a) and (b) are COVID-19 positive case in PNG format and negative case in JPEG format from the original CT scan respectively. Specialists usually identify COVID-19 patients by means of the light grey tissue pointed by arrows in Subfigure (a) of Figure 7.

In the digital image processing field, given a set of possible gray levels or colors and a (rectangular) grid, a digital image attributes a gray value (i.e., brightness) or a color (i.e., hue, saturation and brightness) to each of the grid points or pixels (Suetens, 2017). Therefore, a 2D grayscale image can be represented as a matrix, in which the numbers of row and column represent the height and width of the image, and each entry represents the pixel value ranging from 0 to 255. Typically, zero is taken to be black and 255 is taken to be white, that is, the larger the pixel value, the more intense brightness. This can be illustrated by Subfigures (c) and (d) in Figure 7. Subfigure (c) shows a locally enlarged region pointed by the right red arrow in Subfigure (a). Subfigure (d) is a heatmap of the pixel value of Subfigure (c). It can be seen that the brighter the original region is, the larger pixel value it has. By contrast, the darker the original region is, the smaller pixel value it has. In our analysis, we read the grayscale image by R package `EBImage`. Each pixel value of the image is divided by 255 which rescales the pixel value to $[0,1]$ and the image is upsampled or downsampled into a unified size (height, width) = (150, 150). As a result, we have $\{Y_i, \mathbf{X}_i\}$, where $i = 1, \dots, 746$. Let $Y_i = 1$ indicate a positive case and $Y_i = 0$ the negative case, and $\mathbf{X}_i \in \mathbf{R}^{150 \times 150}$ represents the CT scan image of subject i .

We compare the performance of MVlogistic (Hung and Wang, 2013), CPTR (Zhou et al., 2013) with $R = 2$, SVDTR (Zhou and Li, 2014), TTR (Li et al., 2018) with $(R_1, R_2) = (1, 2)$ and FamGLM. We first combine the training set, validation set and test set provided by the authors, and randomly split the whole data set into training set and validation set with the ratio of 9:1. Then the tuning parameters are determined on the validation set. Next, we evaluate the performance of all models on the training set using five fold cross validation. The mean value of the metrics is recorded as the evaluation metric. The procedure is repeated 50 times.

In order to give a direct illustration of what the factor analysis modeling procedure extracts from the CT images, i.e., the latent factor score matrices, we display four subplots in Figure 8. We use the combined data set to estimate \mathbf{R}, \mathbf{C} and $\{\mathbf{Z}_i\}_{1 \leq i \leq 746}$. The upper row displays the heatmaps of the original CT images of a COVID-19 patient and a normal person ((a) and (b) respectively), and the bottom row displays the heatmaps of reconstructed CT images of (a) and (b) respectively using the estimated factor loading matrices $\hat{\mathbf{R}}$ and $\hat{\mathbf{C}}$, and the corresponding $\hat{\mathbf{Z}}_i$. It can be observed visually that the reconstructed images produce highly morphologically similarity compared with the original images, which manifests that the extracted latent factor score matrices are effective features that can represent the original images to perform subsequent estimation and prediction.

In Table 3, FamGLM outforms other four methods in all four metrics. FamGLM is the only one whose CA score surpasses 0.7. For the Kappa coefficient, FamGLM is the only one that surpasses 0.4 and reaches moderate interrater reliability, while others are below 0.4 and at most can reach the fair level. For sensitivity, all methods are good, while FamGLM and MVlogistic are comparable. For the AUC metric, FamGLM performs better than others, and SVDTR can also reach moderate accuracy though. We also use another model-wide evaluation measure called PR curve to assess the proposed working model, which draws precision against recall (sensitivity). In Figure 9, the PR curves of five modeling methods are

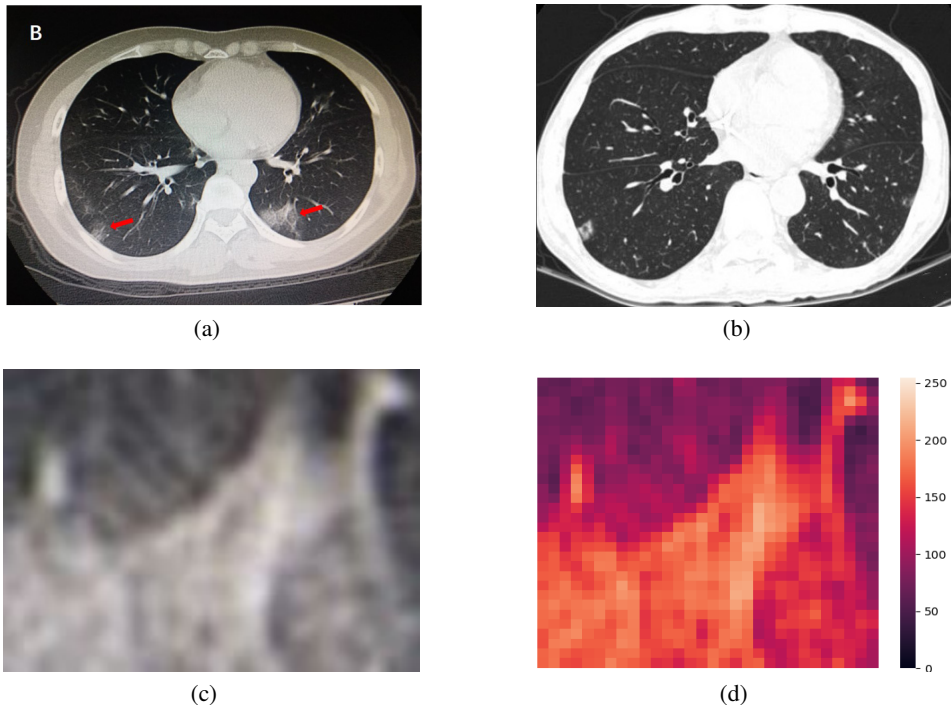


FIG 7. (a): COVID-19 pneumonia with typical imaging features according to the Radiological Society of North America (RSNA) chest CT classification system (Kwee and Kwee, 2020); (b): CT Images of a non-COVID patient. (c): The locally enlarged region pointed by the right red arrow in Subfigure (a). (d): The heatmap of the pixel value of Subfigure (c). The brighter the original region is, the larger pixel value it has. The darker the original region is, the smaller pixel value it has.

illustrated respectively. The precision of all five methods is above 0.5 approximately, which means that all of them have practical utility. It can be seen that the PR curve of FamGLM bulges most towards the upper right corner and achieves a notably better discriminant performance compared to other methods. When recall ranges from 0.4 to 0.85, FamGLM has the highest precision, thus resulting in a higher PR curve; meanwhile, when recall moderately varies from 0.4 to 0.85, precision also varies moderately from 0.5 to 0.85. SVDTR also has a convex hull between recall values 0.55 to 0.8 in the PR curve that is inferior to FamGLM.

TABLE 3
The means (standard errors) of classification metrics on real COVID-CT data with 50 replicates of five-fold cross validations.

	CA	Kappa	Sensitivity	AUC
FamGLM	0.729 (0.016)	0.449 (0.032)	0.669 (0.027)	0.785 (0.017)
MVlogistic	0.692(0.009)	0.381(0.017)	0.657(0.013)	0.742(0.006)
SVDTR	0.681(0.007)	0.360(0.014)	0.643(0.010)	0.755(0.005)
TTR	0.550(0.018)	0.100(0.036)	0.541(0.028)	0.564(0.024)
CPTR	0.535(0.019)	0.070(0.038)	0.529(0.026)	0.545(0.022)

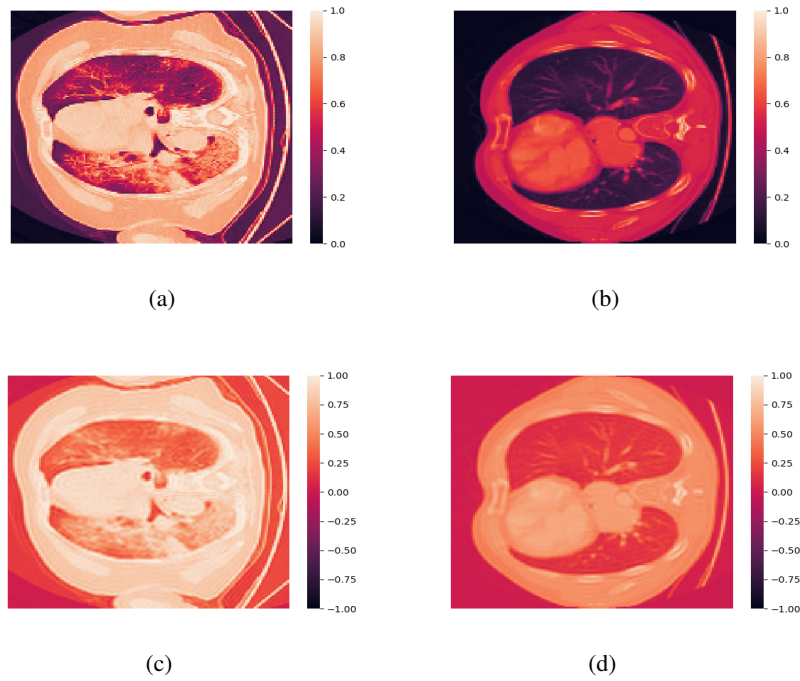


FIG 8. The upper row displays two heatmaps of the original CT images. (a): the CT image of a COVID-19 patient; (b): the CT image of a normal person. The bottom row displays the heatmaps of reconstructed CT images using extracted latent factor score matrices of (a) and (b) respectively.

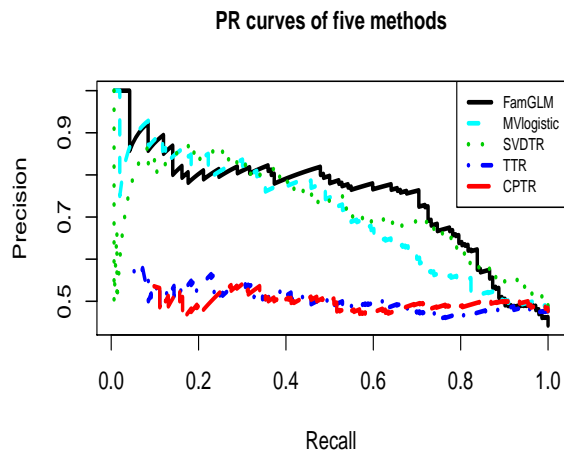


FIG 9. PR (precision against recall (sensitivity)) curves of five methods, including FamGLM (in black solid line), MVlogistic (in cyan dashed line), SVDTR (in green dotted line), TTR (in blue dash-dotted line) and CPTR (in red long dashed line).

5. Discussion. When one converts the generalized linear model into a tensor regression, the tensor regression coefficients need to be estimated accurately; otherwise, the model prediction will be severely impacted. Nevertheless, FamGLM can achieve powerful prediction

capability without concerning the accuracy of estimation of the coefficients of the latent factor regressor. This phenomenon can be well explained through a mathematical way under the linear regression model,

$$Y_i = \alpha^\top \text{vec}(\mathbf{Z}_i) + \epsilon_i, i = 1, \dots, n.$$

Denote

$$\mathcal{Z} = (\text{vec}(\mathbf{Z}_1), \dots, \text{vec}(\mathbf{Z}_n))^\top, \mathbf{Y} = (Y_1, \dots, Y_n)^\top.$$

Then the least squares estimator $\tilde{\alpha} = (\mathcal{Z}^\top \mathcal{Z})^{-1} \mathcal{Z}^\top \mathbf{Y}$ when \mathcal{Z} is known. Noting that in the latent factor model (2), we use the matrix factor score $\hat{\mathbf{Z}}$ rather than \mathcal{Z} to build our latent factor regression. Therefore the real coefficient estimate is

$$\hat{\alpha} = (\hat{\mathcal{Z}}^\top \hat{\mathcal{Z}})^{-1} \hat{\mathcal{Z}}^\top \mathbf{Y}.$$

The matrix factor score $\hat{\mathbf{Z}}_i$ is not a direct estimator for \mathbf{Z}_i but up to two orthogonal matrix multipliers \mathbf{H}_1 and \mathbf{H}_2 . Indeed, $\hat{\mathbf{Z}}_i$ is approximate to the bilinear form of \mathbf{Z}_i under some assumptions (Chen and Fan, 2021; Yu et al., 2021). The strict mathematical representation is

$$\hat{\mathbf{Z}}_i - \mathbf{H}_1^\top \mathbf{Z}_i \mathbf{H}_2 = o_p(1) \mathbf{1}_{k_1 \times k_2},$$

where $\mathbf{1}_{k_1 \times k_2}$ is a matrix of dimension $k_1 \times k_2$ with all entries being 1. Equivalently, it can be denoted by the $\text{vec}(\cdot)$ operator in the form

$$\text{vec}(\hat{\mathbf{Z}}_i) = (\mathbf{H}_2 \otimes \mathbf{H}_1)^\top \text{vec}(\mathbf{Z}_i) + o_p(1) \mathbf{1}_{k_1 k_2},$$

where $\mathbf{A} \otimes \mathbf{B}$ is the Kronecker product of matrices \mathbf{A} and \mathbf{B} , and $\mathbf{1}_{k_1 k_2}$ is a column vector of length $k_1 k_2$ with all entries being 1. Consequently, we have the estimate $\hat{\alpha}$ and the prediction \hat{Y}_i

$$\hat{\alpha} = (\mathbf{H}_2 \otimes \mathbf{H}_1)^\top \tilde{\alpha} + o_p(1) \mathbf{1}_{k_1 k_2}, \hat{Y}_i = \hat{\alpha}^\top \text{vec}(\hat{\mathbf{Z}}_i) = \tilde{\alpha}^\top \text{vec}(\mathbf{Z}_i) + o_p(1).$$

respectively. Apparently, we focus on the prediction since its accuracy is guaranteed by the aforementioned probabilistic procedure and we skip the interim coefficient estimation and evaluation.

We may consider two tracks of extension of FamGLM. One is to extend FamGLM to handle regressors including the tensor-valued predictor. Based on the latest tensor factor model in time series (Chen et al., 2021), the extracted tensor factor scores can be used to form the latent tensor regression. What will be challenging is to develop a new estimation procedure and algorithm for independent tensor variates wearing off the temporal dependency under the multiway volume effects of tensor structure. The other is to model and derive estimation for regression with both matrix-valued predictor \mathbf{X} and matrix-valued response \mathbf{Y} from the insight of matrix factor modeling, where both \mathbf{X} and \mathbf{Y} possess characteristics of high dimension. If \mathbf{Y} is continuous, we can adopt the nonlinear interaction matrix factor model for both $\mathbf{Y} = \mathbf{AFL}^\top + \mathbf{E}_\mathbf{Y}$ and $\mathbf{X} = \mathbf{RZC}^\top + \mathbf{E}_\mathbf{X}$. Then it comes out the general multivariate multiple regression $\text{vec}(\mathbf{F}) = \mu + \mathbf{B}\text{vec}(\mathbf{Z}) + \epsilon$.

Acknowledgments. The authors would like to thank the anonymous referees, an Associate Editor and the Editor for their constructive comments that improved the quality of this paper.

Funding. Zhang Yuzhe’s research is supported by the postgraduate studentship of USTC. Zhang Xu’s research is partly supported by the National Natural Science Foundation of China (12171167). Zhang Hong’s research is partly supported by the National Natural Science Foundation of China (11771096, 7209121, 12171451). Liu Catherine’s research is partly supported by General Research Funding (15301519), RGC, HKSAR.

REFERENCES

- Bai, J. (2003). Inferential theory for factor models of large dimensions. *Econometrica*, 71(1):135–171.
- Beck, A. and Teboulle, M. (2009). A fast iterative shrinkage-thresholding algorithm for linear inverse problems. *SIAM journal on imaging sciences*, 2(1):183–202.
- Caffo, B. S., Crainiceanu, C. M., Verduzco, G., Joel, S., Mostofsky, S. H., Bassett, S. S., and Pekar, J. J. (2010). Two-stage decompositions for the analysis of functional connectivity for fMRI with application to Alzheimer’s disease risk. *NeuroImage*, 51(3):1140–1149.
- Chen, E. Y. and Fan, J. (2021). Statistical inference for high-dimensional matrix-variate factor models. *Journal of the American Statistical Association*, pages 1–18.
- Chen, R., Yang, D., and Zhang, C. (2021). Factor models for high-dimensional tensor time series. *Journal of the American Statistical Association*, pages 1–23.
- Ding, S. and Cook, R. (2018). Matrix variate regressions and envelope models. *Journal of the Royal Statistical Society: Series B (Statistical Methodology)*, 80(2):387–408.
- Ding, S. and Cook, R. D. (2014). Dimension folding PCA and PFC for matrix-valued predictors. *Statistica Sinica*, 24(1):463–492.
- Fang, J. and Yi, G. Y. (2021). Matrix-variate logistic regression with measurement error. *Biometrika*, 108(1):83–97.
- Hung, H. and Wang, C.-C. (2013). Matrix variate logistic regression model with application to eeg data. *Bio-statistics*, 14(1):189–202.
- Jiang, B., Petkova, E., Tarpey, T., and Ogden, R. T. (2020). A bayesian approach to joint modeling of matrix-valued imaging data and treatment outcome with applications to depression studies. *Biometrics*, 76(1):87–97.
- Kapoor, V., McCook, B. M., and Torok, F. S. (2004). An introduction to PET-CT imaging. *Radiographics*, 24(2):523–543.
- Kolda, T. G. and Bader, B. W. (2009). Tensor decompositions and applications. *SIAM Review*, 51(3):455–500.
- Kwee, T. C. and Kwee, R. M. (2020). Chest CT in COVID-19: what the radiologist needs to know. *RadioGraphics*, 40(7):1848–1865.
- Lam, C. and Yao, Q. (2012). Factor modeling for high-dimensional time series: inference for the number of factors. *The Annals of Statistics*, 40(2):694–726.
- Lange, K., Chambers, J., and Eddy, W. (2010). *Numerical analysis for statisticians*, volume 1. Springer.
- Lawley, D. N. and Maxwell, A. E. (1962). Factor analysis as a statistical method. *Journal of the Royal Statistical Society: Series D (The Statistician)*, 12(3):209–229.
- Li, B., Kim, M. K., Altman, N., et al. (2010). On dimension folding of matrix-or array-valued statistical objects. *The Annals of Statistics*, 38(2):1094–1121.
- Li, C. and Zhang, H. (2021). Tensor quantile regression with application to association between neuroimages and human intelligence. *The Annals of Applied Statistics*, 15(3):1455 – 1477.
- Li, L. and Zhang, X. (2017). Parsimonious tensor response regression. *Journal of the American Statistical Association*, 112(519):1131–1146.
- Li, X., Xu, D., Zhou, H., and Li, L. (2018). Tucker tensor regression and neuroimaging analysis. *Statistics in Biosciences*, 10(3):520–545.
- Liu, C., Liu, A., and Halabi, S. (2011). A min–max combination of biomarkers to improve diagnostic accuracy. *Statistics in Medicine*, 30(16):2005–2014.
- Suetens, P. (2017). *Fundamentals of medical imaging*. Cambridge university press.
- Wang, D., Liu, X., and Chen, R. (2019). Factor models for matrix-valued high-dimensional time series. *Journal of Econometrics*, 208(1):231–248.
- Yang, X., He, X., Zhao, J., Zhang, Y., Zhang, S., and Xie, P. (2020). COVID-CT-Dataset: a CT image dataset about COVID-19. *arXiv preprint arXiv:2003.13865*.
- Ye, J. (2005). Generalized low rank approximations of matrices. *Machine Learning*, 61(1-3):167–191.
- Yu, L., He, Y., Kong, X., and Zhang, X. (2021). Projected estimation for large-dimensional matrix factor models. *Journal of Econometrics*.
- Zare, A., Ozdemir, A., Iwen, M. A., and Aviyente, S. (2018). Extension of pca to higher order data structures: An introduction to tensors, tensor decompositions, and tensor pca. *Proceedings of the IEEE*, 106(8):1341–1358.
- Zhou, H. and Li, L. (2014). Regularized matrix regression. *Journal of the Royal Statistical Society: Series B (Statistical Methodology)*, 76(2):463–483.
- Zhou, H., Li, L., and Zhu, H. (2013). Tensor regression with applications in neuroimaging data analysis. *Journal of the American Statistical Association*, 108(502):540–552.